arXiv:1210.8377v1 [cond-mat.str-el] 31 Oct 2012

Engineering Degeneracy: a Critical Ground State for Artificial Spin Ice

Gia-Wei Chern[1], Muir J. Morrison[1], and Cristiano Nisoli[1]
[1] *Theoretical Division and Center for Nonlinear Studies, LANL, Los Alamos, NM 87545, USA*

(Dated: November 1, 2012)

The constraints of a realistic magnetic interaction limit the possibility of realizing degenerate vertex models with artificial spin ice in two dimensions. Here we present and study a novel vertex-frustrated geometry which exhibits a residual entropy density. While interesting in its own regard as a new form of frustration in a vertex system, our lattice opens new pathways for implementing degeneracy in artificial magnetic nanoarrays, a task so far elusive. We demonstrate that its degenerate ground state can be mapped to the disordered phase of the exactly solvable F-model. Monte Carlo simulations extend our study to thermal states, and, significantly, find algebraic correlations for frustrated vertices, magnetic charges, and spins in the ground state, pointing to a critical phase.

Artificial Spin Ice (ASI) has raised considerable interest for its technological potentials, and as a tailorable medium to investigate novel collective phenomena in a materials-by-design approach [1–18]. ASI was inspired by the so-called spin ice compounds [19, 20], a special class of pyrochlore ferromagnets in which the magnetic interactions resemble the frustrated proton ordering in water ice [21–23]. Both water ice and spin ice retain a finite entropy density even at very low temperatures. The local spin arrangement in spin ice is dictated by rules similar to the Bernal-Fowler ice rules [21]. An interesting consequence of this local ordering is the appearance of algebraically decaying spin correlations [24], similar to those in two-dimensional (2D) lattice systems with hard-core constraints such as dimer or vertex models [25].

The original artificial spin ice presented by Wang *et al.* consists of magnetically interacting elongated permalloy nanoislands arranged as links of a square lattice [1, 3, 4]. Within the nearest-neighbor approximation, the square ice can be mapped to a non-degenerate six-vertex model: the anisotropic nature of the magnetic interaction in a 2D arrangement lifts the degeneracy of the six distinct 2-in-2-out vertices and the ground state is described by the ordered phase of the F-model [25]. Ways to overcome this limit and induce degeneracy have been proposed [26] yet they present challenges in nanofabrication.

So far, kagome ice, in which the islands are arranged along the edges of a honeycomb lattice [12–14], is the only ASI of extensive degeneracy, inheriting residual entropy from its six low-energy 2-in-1-out or 1-in-2-out degenerate vertices (pseudo-ice rule). However this pseudo-ice regime is non-critical, with exponentially-decaying spin correlation [31]. Recently Morrison and coworkers have proposed "vertex-frustrated lattices" for ASI. The residual entropy in these systems emerges from the inability of allocating all the vertices in their lowest energy configuration, rather than from a degeneracy at the vertex level [15].

Here we present the first comprehensive study of a particularly interesting vertex-frustrated lattice depicted in Fig. 1(a). This so-called shakti lattice is maximally vertex-frustrated [15]: on each minimal loop, at least one vertex is not in its lowest energy configuration. Remarkably, we find that its residual entropy can be computed exactly by mapping the $T = 0$ manifold of the shakti spin-ice into a disordered state of the non-degenerate F-model. The degeneracy implied by topological frustration can be subsumed as a fictitious temperature for a non-degenerate vertex model. We also show numerically that its correlations are algebraic, indicating a critical ground state.

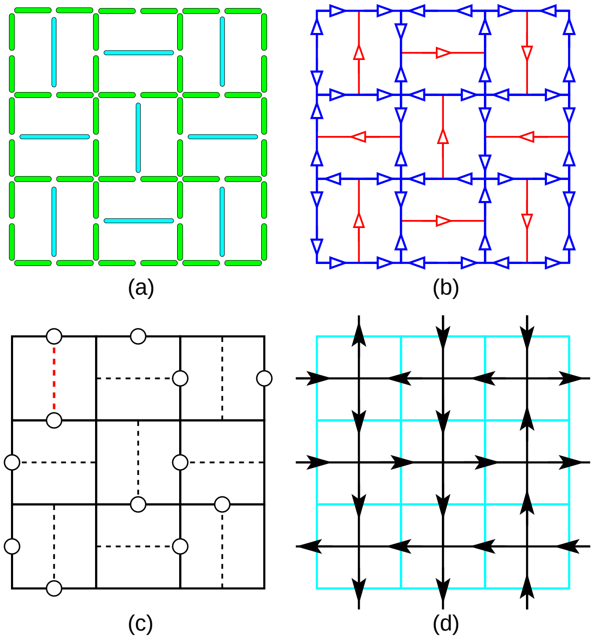

FIG. 1: (Color online) (a) The lattice geometry of the shakti spin ice. The spin-ice state and the corresponding defect-vertex configuration in a typical disordered ground state are shown in panels (b) and (c), respectively. The defect type-II' vertices are indicated by circles. The defect configuration is further mapped to an emergent 6-vertex model in (d).

The shakti lattice can be derived from the square lattice [1] by alternatively placing an additional vertical or horizontal permalloy island in each square plaquette. The resulting lattice consists of vertices with both coordination numbers $z = 4$ and 3, as in Fig. 2. The perpendic-

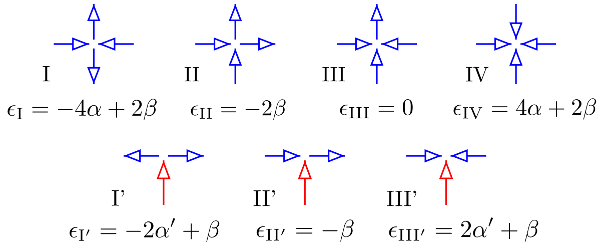
I
II
III
IV
$\epsilon_{\rm I} = -4\alpha + 2\beta$
$\epsilon_{\rm II} = -2\beta$
$\epsilon_{\rm III} = 0$
$\epsilon_{\rm IV} = 4\alpha + 2\beta$
I'
II'
III'
$\epsilon_{\rm I'} = -2\alpha' + \beta$
$\epsilon_{\rm II'} = -\beta$
$\epsilon_{\rm III'} = 2\alpha' + \beta$

FIG. 2: (Color online) The seven different types of vertices in artificial spin ice shown in Figs. 1(a) and (b). Also shown is the magnetostatic energy of the vertices expressed in terms of three parameters α, α', and β. The multiplicities of the various vertex types are: $q_{\rm I} = 2$, $q_{\rm II} = 4$, $q_{\rm III} = 8$, and $q_{\rm IV} = 2$ for $z = 4$ vertices, and $q_{\rm I'} = 2$, $q_{\rm II'} = 4$, and $q_{\rm III'} = 2$ for $z = 3$ vertices.

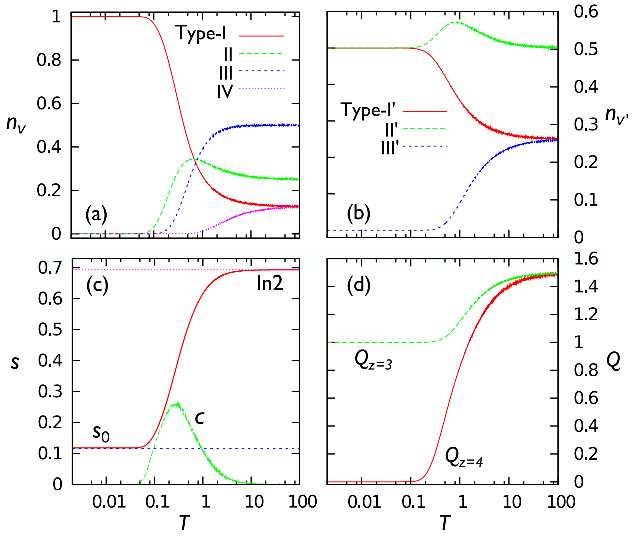

FIG. 3: (Color online) Monte Carlo simulation of the shakti spin ice with $N_s = 1000$ spins. Parameters $\alpha = \alpha' = 1.41\beta$ and periodic boundary conditions are used in the simulations. (a) and (b) show the fraction of various vertex types as a function of temperature T measured in units of $\epsilon_d = \mu_0\mu^2/4\pi a^3$. (c) shows the temperature dependence of entropy density s and specific-heat c. The entropy curve $s(T)$ is obtained by integrating the specific-heat $c(T)/T$. The averaged magnitude of magnetic charge (in natural units) at the $z = 3$ and 4 vertices is shown in (d).

ular geometry of the islands around the $z = 3$ sites breaks the six-fold degeneracy of the 2-in-1-out/1-in-2-out vertices. A new type of frustration arises from the fact that not all $z = 3$ vertices can assume the minimum-energy configurations simultaneously.

In this paper we limit ourselves to a vertex-model of the shakti lattice, which has proved useful in describing experimental results in ASI [1, 3, 4]. Energetically, there are four distinct vertex types, labeled by numerals I–IV, for the $z = 4$ sites, while the three types of $z = 3$ vertices are labeled as type I', II', and III'. The dominant nearest-neighbor interaction energy can be parameterized by α and β, the magnetostatic energy between two islands in perpendicular and parallel geometries, respectively, at the $z = 4$ vertex, and α' represents the energy between a pair of perpendicular island at the $z = 3$ vertex. In terms of these parameters, the various vertex energies are summarized in Fig. 2.

Since the energies $\alpha > \beta$ in 2D, contrary to the pyrochlore spin ice, the degeneracy between the two types (I and II) of 2-in-2-out vertices is lifted. In the case of square ASI, a long-range spin order consisting of a staggered arrangement of the energetically favorable type-I vertices emerges as the ground state.

Approximating each permalloy island as a point-like dipole, simple calculation gives $\alpha = 24\sqrt{2}$, $\beta = 16$, and $\alpha' = x\,(384/25\sqrt{5})$ measured in units of $\epsilon_d = \mu_0\mu^2/4\pi a^3$, where μ and $x\mu$ are the effective dipole moments of the blue and red spins, respectively, and a is the lattice constant. The geometry and size of the red spins thus determine which vertex type (I' or II') has lower energy. As can be easily checked, an energetically favorable type-II' vertex gives rise to a long-range spin order in the shakti lattice. In the following, we mainly concern ourselves with the more interesting case in which $\epsilon_{\rm I'} < \epsilon_{\rm II'}$.

Ideally the ground state of the spin ice is reached when the individual vertex assumes either type-I or I' configurations depending on its coordination number [15]. However, the special geometry of the lattice precludes such an ideal arrangement [15]. Assuming $\alpha' \sim \alpha$, the type-II' is the next favorable vertex energetically. Consequently, the ground state is expected to contain only the two minimum-energy vertices (I and I') and the next lowest-energy type-II' vertices.

To investigate the thermodynamic behavior of the shakti spin ice as a vertex model, we first perform Monte Carlo simulations. The results shown in Figs. 3 are obtained assuming nearest-neighbor interaction with parameters $\alpha = \alpha' = 1.41\beta$. At high temperatures the system is in an uncorrelated paramagnetic phase as the population of various vertex types reaches an equilibrium according to their respective multiplicities. On the other hand, as temperature tends to zero, the magnet is indeed dominated by vertices of types I, I', and II'. The crossover between these two regimes is marked by a broad peak in the specific-heat [Fig. 3(c)]. The presence of ice rules at low T is confirmed by the temperature dependence of averaged magnetic charges at individual vertex shown in Fig. 3(d). The 2-in-2-out rule indicates a vanishing magnetic charge $Q = 0$ at the $z = 4$ vertices while the 1-in-2-out/2-in-1-out rule implies a magnetic charge $Q = \pm 1$ at the $z = 3$ vertices.

By fixing the high-T entropy density to $k_B \ln 2$, we find a residual entropy $s_0 \approx 0.1178\,k_B$ per spin from the simulations. This nonzero entropy density implies an extensive degeneracy of spin-ice states at low temperatures. Below the crossover, we notice that the only vertex types with nonzero fractional populations are $n_{\mathrm{I}} = 1$, $n_{\mathrm{I'}} = n_{\mathrm{II'}} = 1/2$: while all $z = 4$ sites are minimum-energy type-I vertices, only half of the $z = 3$ vertices are in the ground state. The other half are frustrated type-II' vertices. We can thus use locations of the frustrated vertices to characterize the spin-ice states; these unhappy vertices will be referred to as defects for simplicity. For example, Figs. 1(b) and (c) show a generic disordered spin-ice state and the corresponding defect configuration, respectively. It should be noted that this mapping is at least 2-to-1: each spin-ice state and its time-reversal partner are mapped to the same defect configuration. For square plaquette with defects sitting at the two ends of the center spin, i.e. type-6 plaquette in Fig. 4, there is an additional Z_2 degree of freedom associated with the direction of the center (red) spin.

To understand the structure of the degenerate spin-ice manifold, we first note that each plaquette has at least two defects in any spin-ice state; this can be easily demonstrated by enumerating all possible magnetic configurations in a plaquette [15]. As a result, any configuration in which each plaquette has *exactly* two defects is a ground state, consistent with the numerical result that $n_{\mathrm{II'}} = 1/2$ as $T \to 0$. This two-defects constraint is similar to the 2-in-2-out ice rule in square ice. Fig. 4 shows the six different two-defects configurations in a plaquette. Since there are two types of plaquette in our lattice with different orientations of the center island, those with vertical (horizontal) center spin are referred to in the following as type-A (B) plaquettes.

Noting that the centers of plaquettes in our model form a square lattice, it is not surprising that each defect configuration can be mapped to a 6-vertex state. To establish this mapping, we draw an arrow from type-A to its neighboring type-B plaquette if their common edge contains a defect vertex. On the other hand, an edge without defect vertex corresponds to an arrow pointing from type-B to type-A plaquette. This establishes an one-to-one mapping between the two-defects plaquettes and the 2-in-2-out vertices; see Fig. 4. An example of the mapping is also illustrated in Fig. 1(d).

We now consider the partition function of the emergent 6-vertex model. As discussed above, In addition to the global Z_2 time-reversal symmetry, there are two different spin states corresponding to type-6 vertex. This additional doublet degeneracy comes from the fact that the direction of center spin can be parallel or anti-parallel to the orientation of the center island [Fig. 4(f)]. Let n_6 denote the number of type-6 vertex in a given 6-vertex configuration $\mathcal{C}$, the ground-state partition function of the shakti spin ice is simply

$$Z = \sum_{\mathcal{C}} 2^{n_6} = \sum_{\mathcal{C}} \big(\sqrt{2}\big)^{n_5+n_6}, \tag{1}$$

The second identity holds when periodic or cylindrical boundary conditions are imposed. This is because type-5 and 6 vertices are sources and sinks, respectively, of the horizontal arrows or 'fluxes'. As the total flux is conserved, there must be as many sinks as sources, i.e. $n_5 = n_6$ [25]. The degeneracy of Eq. (1) can be estimated as: $W = W_{\mathrm{ice}} \times 2^{N_\square \langle n_6 \rangle}$, where $W_{\mathrm{ice}} = \left(\frac{4}{3}\right)^{3N_\square/10}$ is the degeneracy of the ideal square ice [25], $\langle n_6 \rangle \sim 0.189$ is the average population of type-6 vertex in a ice state, and $N_\square$ is the number of plaquettes (or vertices in a 6-vertex state). Since $N_\square = N_s/5$ in shakti ice, where N_s is the number of spins, this gives a residual entropy density $s_0 = k_B \ln W/N_s \sim 0.1125 k_B$, which is close to the numerical result.

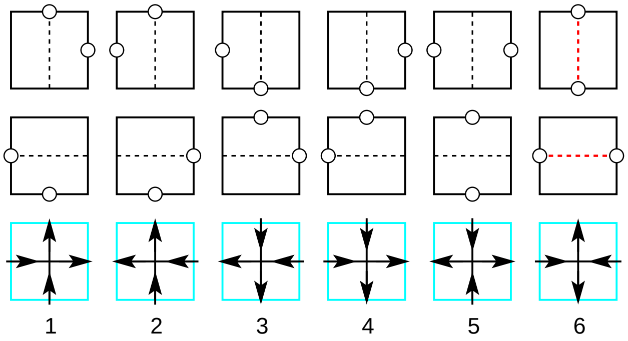

FIG. 4: (Color online) The six possible two-defects configurations in a plaquette (for both type-A and B) and their mapping to the 2-in-2-out vertices.

The entropy density of the shakti spin-ice can be exactly computed by recasting the partition function (1) into that of the standard F-model [27]:

$$Z = \sqrt{2}^{N_\square}\, Z_F = \sqrt{2}^{N_\square} \sum_{\mathcal{C}} \prod_{i=1}^{6} \omega_i^{n_i}, \tag{2}$$

where ω_i denotes the statistical weight of the type-i vertex: $\omega_1 = \omega_2 = \omega_3 = \omega_4 = e^{-K}$ and $\omega_5 = \omega_6 = 1$. The case of shakti ice corresponds to $K = \frac{1}{2}\ln 2$.

For a general F-model, the parameter $K \geq 0$ acts as an inverse temperature; the square ice corresponds to the special case with $K = 0$ or infinite T. It is known that a Kosterlitz-Thouless transition occurs at $K_c = \ln 2$ [25]. The correlation length is finite in the ordered state for $K > K_c$, while the system remains critical with an infinite correlation length for $K \leq K_c$. Our case with $K = K_c/2$ thus corresponds to a critical phase with disordered vertices and spins.

The residual entropy of Eq. (2) is $S/k_B = \ln Z = (N_\square/2)\ln 2 + \ln Z_F$. The entropy density of the F-model with $K = K_c/2$ can be exactly computed using the Bethe *ansatz* [27]. We thus obtain a residual entropy density for the shakti ice:

$$\frac{S}{N_\square\, k_B} = \frac{1}{\pi}\int_0^{\frac{\pi}{2}} \ln\cot(k/2)\, dk = \frac{2G}{\pi} = 0.583122, \tag{3}$$

where G is the Catalan's constant [27]. Since the number of spins $N_s = 5N_\square$ in shakti ice, Eq. (3) corresponds to

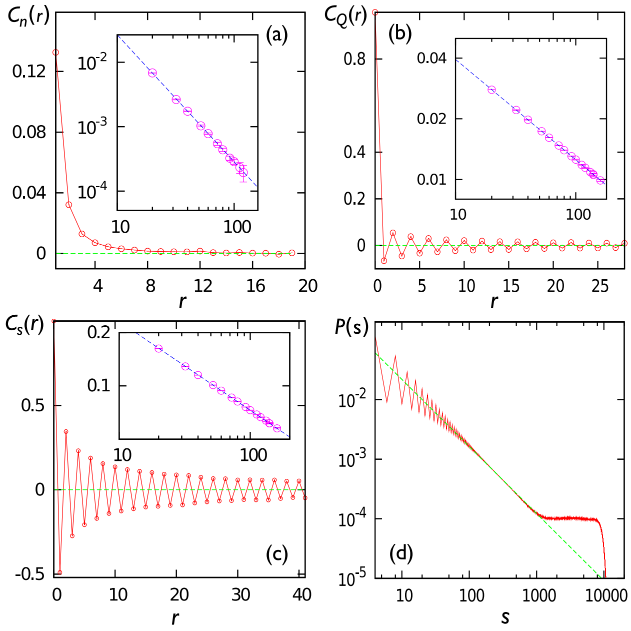

FIG. 5: (Color online) The correlation function for (a) defect-vertex, (b) magnetic charge, and (c) magnetic moment obtained from Monte Carlo simulations using the loop algorithm [28]. These correlations are measured between defects, charges, or spins at the vertical edges of two plaquettes separated by r unit cells along the diagonal direction of the lattice. The insets show the same data (with absolute values) in log-log plot. Panel (d) shows the probability distribution of loop lengths s.

an entropy density per spin $S/N_s\, k_B = 0.116624$, which is fairly close to the numerically estimated value $s_0 = 0.1178 k_B$ [Fig. 3(c)].

We now turn to the correlation functions in the ground state. To efficiently navigate between different six-vertex states, we use the loop algorithm in which detailed balance is always satisfied locally when constructing the loops [28, 29]. We first consider the defect-defect correlation function $C_n(\mathbf{r}) = \langle \delta n(\mathbf{r})\, \delta n(0) \rangle$, where $\delta n(\mathbf{r}) = n(\mathbf{r}) - \langle n \rangle$, and $n(\mathbf{r}) = 1$ or 0 dependeing on the presence or absence of defect vertex at edge $\mathbf{r}$. The average defect density $\langle n \rangle = 1/2$ is consistent with the constraint that each plaquette has two defects in the ground state. The correlation function $C_n(r)$ along the diagonal direction of the lattice, shown in Fig. 5(a), falls off quickly beyond a few lattice constants. As expected for correlations in a critical state, the inset log-log plot shows a power-law decaying $C_n(r) \sim r^{-\eta_n}$ with an estimated exponent $\eta_n = 1.96986 \pm 0.0046$.

As in the kagome ice case, there is a residual magnetic charge $Q = \pm 1$ at the $z = 3$ vertices [also see Fig. 3(d)]. The local arrangement of charges also follows certain rules: charges of the same sign always occur at the two ends of the center vertical or horizontal island in type-1 to 4 plaquettes, while opposite charges always occupy the two ends of the center island in a type-5 or 6 plaquette. Fig. 5(b) shows a stronger charge-charge correlation $C_Q(\mathbf{r}) = \langle Q(\mathbf{r})\, Q(0) \rangle$ than that of defect vertices. Again, we find an algebraic correlation $C_Q(r) \sim r^{-\eta_Q}$ at large separation with $\eta_Q = 0.497144 \pm 0.001952$.

Since the mapping to defects configuration in a plaquette and the corresponding 6-vertex state is at least 2-to-1, the magnetic state of a plaquette is determined by its vertex type and an Ising variable. For a given 6-vertex state $\mathcal{C}$, these Ising variables are not uniform and have to be determined consistently by first fixing spins at the boundaries. The numerically obtained spin-spin correlation function is shown in Fig. 5(c). Its power-law decay $C_s(r) \sim r^{-\eta_s}$ has an exponent $\eta_s = 0.502075 \pm 0.002028$.

The lack of a length scale in a critical phase implies that loops of all lengths will be found in any given state. To see this we numerically evaluate the probability distribution function $P(s)$ of loop length s; the result is shown in Fig. 5(d). Similar to loops in square or pyrochlore ices [30], the loop statistics exhibits two distinct regimes: a power-law distribution $P(s) \sim s^{-1.125}$ for short loops and a flat distribution due to winding loops in a finite system.

In summary, we have proposed a novel artificial spin ice characterized by frustrated ordering of defect vertices in the ground state. The resulting degenerate manifold can be mapped to a special 6-vertex F-model and solved exactly. We have also solved the model numerically and found that in the ground state, correlation functions of frustrated vertices, magnetic charges, and spins exhibit a power-law decay consistent with a critical ground state predicted by the exact solvable F-model. Beside its intrinsic interest as a novel form of frustration which can be mapped into temperature, this system can be easily fabricated as an extensively degenerate ASI, and annealed in its degenerate ground state [5, 16–18], thus opening novel directions in the study of frustration induced degeneracy. In future work we will demonstrate the emergence of a smectic phase corresponding to magnetic monopole crystallization when long range interactions are included.

We thank P. Mellado, A. Libal, C. Reichhardt, and R. Moessner for useful comments. This work was carried out under the auspices of the National Nuclear Security Administration of the U.S. Department of Energy at Los Alamos National Laboratory under Contract No. DEAC52-06NA25396. GWC acknowledges the support of LANL Oppenheimer Fellowship.

[1] R. F. Wang, C. Nisoli, R. S. Freitas, J. Li, W. McConville, B. J. Cooley, M. S. Lund, N. Samarth, C. Leighton, V. H. Crespi, and P. Schiffer, Nature **439**, 303 (2006).
[2] S. T. Bramwell, Nature, **439**, 273 (2006).
[3] C. Nisoli, R. Wang, J. Li, W. F. McConville, F. E. Lammert, P. Schiffer, and V. H. Crespi, Phys. Rev. Lett. **98**, 217203 (2007).

[4] C. Nisoli, J. Li, X. Ke, D. Garand, P. Schiffer, and V. H. Crespi, Phys. Rev. Lett. **105**, 047205 (2010).
[5] J. P. Morgan, A. Stein, S. Langridge, and C. H. Marrows, Nature Phys. **7**, 75 (2011).
[6] G. Möller and R. Moessner, Phys. Rev. B **80**, 140409 (2009).
[7] G.-W. Chern, P. Mellado, and O. Tchernyshyov, Phys. Rev. Lett. **106**, 207202 (2011).
[8] P.E. Lammert, X. Ke, J. Li, C. Nisoli, D. M. Garand, V. H. Crespi, and P. Schiffer, Nature Phys. **6** 786789 (2010).
[9] X. Ke, J. Li, C. Nisoli, P. E. Lammert, W. McConville, R. F. Wang, V. H. Crespi, and P. Schiffer, Phys. Rev. Lett. **101**, 037205 (2008).
[10] E. Mengotti, L. J. Heyderman, A. Bisig, A. Fraile Rodriguez, L. Le Guyader, F. Nolting, and H. B. Braun, J. Appl. Phys. **105**, 113113 (2009).
[11] A. Libál, C. Reichhardt, and C. J. Olson Reichhardt, Phys. Rev. Lett. **97**, 228302 (2006).
[12] M. Tanaka, E. Saitoh, H. Miyajima, T. Yamaoka, and Y. Iye, Phys. Rev. B **73**, 052411 (2006).
[13] Y. Qi, T. Brintlinger, and J. Cumings, Phys. Rev. B **77**, 094418 (2008).
[14] J. Li, X. Ke, S. Zhang, D. Garand, C. Nisoli, P. Lammert, V. H. Crespi, and P. Schiffer, Phys. Rev. B **81**, 092406 (2010).
[15] M. Morrison, T. R. Nelson, C. Nisoli, arXiv:1210.7843.
[16] V. Kapaklis, U. B. Arnalds, A. Harman-Clarke, E. Th. Papaioannou, M. Karimipour, P.Korelis, A. Taroni P. C. W. Holdsworth, S. T. Bramwell, and B. Hjoorvarsson, New J. Phys. **14**, 035009 (2012).
[17] C. Nisoli, New J. Phys. **14** 035017 (2012)
[18] S. J. Greaves and H. Muraoka, J. Appl. Phys. **112**, 043909 (2012)
[19] M. J. Harris, S. T. Bramwell, D. F. McMorrow, T. Zeiske, and K. W. Godfrey, Phys. Rev. Lett. **79**, 2554 (1997).
[20] S. T. Bramwell and M. J. P. Gingras, Science **294**, 1495 (2001).
[21] V. F. Petrenko and R. W. Whitworth, *Physics of ice* (Oxford University Press, 1999).
[22] J. D. Bernal, R. H. Fowler, J. Chem. Phys. **1**, 515 (1933).
[23] L. Pauling, J. Am. Chem. Soc. **57**, 2680 (1935).
[24] C. L. Henley, Annu. Rev. Condens. Matter Phys. **1**, 179 (2010).
[25] R. J. Baxter, *Exactly Solved Models in Statistical Physics* (Academic, New York, 1982).
[26] G. Möller and R. Moessner, Phys. Rev. Lett. **96**, 237202 (2006).
[27] E. H. Lieb, Phys. Rev. Lett. **18**, 1046 (1967); E. H. Lieb and F. W. Wu, *Phase Transitions and Critical Phenomena* (Academic, London, 1971), Vol. 1.
[28] H. G. Evertz, G. Lana, and M. Marcu, Phys. Rev. Lett. **70**, 875 (1993).
[29] O. F. Syljuasen and M. B. Zvonarev, Phys. Rev. E **70**, 016118 (2004).
[30] L. D. C. Jaubert, M. Haque, and R. Moessner, Phys. Rev. Lett. **107**, 177202 (2011).

[31] Inclusion of long range interactions reveals an algebraic ice phase with ordered magnetic charge [6, 7]. However this phase has not been found experimentally yet, and experimental results point to a satisfying approximation of honeycomb ice in terms of a nearest neighbor vertex model [1, 3, 4, 12–14].